A point mutation in the human Slo1 channel that impairs its sensitivity to omega-3 docosahexaenoic acid

Toshinori Hoshi,[1] Rong Xu,[1] Shangwei Hou,[2] Stefan H. Heinemann,[3] and Yutao Tian[1]

[1]Department of Physiology, University of Pennsylvania, Philadelphia, PA 19104
[2]Key Laboratory of Systems Biomedicine, Shanghai Center for Systems Biomedicine, Shanghai Jiao Tong University, Shanghai 200240, China
[3]Department of Biophysics, Center for Molecular Biomedicine, Friedrich Schiller University Jena and Jena University Hospital, D-07745 Jena, Germany

Long-chain polyunsaturated omega-3 fatty acids such as docosahexaenoic acid (DHA) at nanomolar concentrations reversibly activate human large-conductance Ca^{2+}- and voltage-gated K^+ (Slo1 BK) channels containing auxiliary β1 or β4 subunits in cell-free patches. Here we examined the action of DHA on the Slo1 channel without any auxiliary subunit and sought to elucidate the biophysical mechanism and the molecular determinants of the DHA sensitivity. Measurements of ionic currents through human Slo1 (hSlo1) channels reveal that the stimulatory effect of DHA does not require activation of the voltage or Ca^{2+} sensors. Unlike gating of the hSlo1 channel, that of the *Drosophila melanogaster* Slo1 (dSlo1) channel is unaltered by DHA. Our mutagenesis study based on the differential responses of human and dSlo1 channels to DHA pinpoints that Y318 near the cytoplasmic end of S6 in the hSlo1 channel is a critical determinant of the stimulatory action of DHA. The mutation Y318S in hSlo1, which replaces Y with S as found in dSlo1, greatly diminishes the channel's response to DHA with a 22-carbon chain whether β1 or β4 is absent or present. However, the responses to α-linolenic acid, an omegea-3 fatty acid with an 18-carbon chain, and to arachidonic acid, an omega-6 fatty acid with a 20-carbon chain, remain unaffected by the mutation. Y318 in the S6 segment of hSlo1 is thus an important determinant of the electrophysiological response of the channel to DHA. Furthermore, the mutation Y318S may prove to be useful in dissecting out the complex lipid-mediated modulation of Slo1 BK channels.

INTRODUCTION

Dietary fats in the form of triglycerides are broken down by lipase in the small intestine, and released free fatty acids are then absorbed into the body. Among the diverse fatty acids, long-chain polyunsaturated omega-3 fatty acids play particularly critical roles in human health (Uauy and Dangour, 2006). Dietary intake of these omega-3 fatty acids, enriched in oily fish, is postulated to have a wide array of health-promoting effects (Saravanan et al., 2010; Mozaffarian and Wu, 2011). For example, the omega-3 fatty acids docosahexaenoic acid (DHA; 22:6(ω-3)), with a 22-carbon chain, and eicosapentaenoic acid (EPA; 20:5(ω-3)), with a 20-carbon chain, may promote healthy cardiovascular function (Ramel et al., 2010; Saravanan et al., 2010; Liu et al., 2011), although recent studies have not yielded unequivocal results (Rizos et al., 2012; Roncaglioni et al., 2013), and some undesirable correlations have been reported in a different organ system (Brasky et al., 2013). The underlying mechanisms of the purported beneficial effects of omega-3 fatty acids are beginning to be investigated, and one of the critical tasks is to identify the molecular targets of these fatty acids. An early effort has revealed that the G protein–coupled receptor 120 involved in the inflammatory response (Oh et al., 2010; Yan et al., 2013) and weight control (Ichimura et al., 2012) is directly activated by DHA with an EC_{50} of ∼10 μM (Oh et al., 2010). This interaction may contribute to the physiological role of omega-3 fatty acids in the inflammatory process (Im, 2012; Flock et al., 2013; Orr et al., 2013).

Large-conductance Ca^{2+}- and voltage-gated K^+ (Slo1 BK, maxiK, or $K_{Ca}1.1$) channels are allosterically activated by intracellular Ca^{2+} and membrane depolarization (Horrigan and Aldrich, 2002; Hoshi et al., 2013a). Slo1 BK channels play important roles in the regulation of numerous physiological processes, including regulation of vascular tone (Nelson and Quayle, 1995; Brenner et al., 2000b), and the channels are well known for their rich repertoire of modulation by multitudes of cellular signaling molecules (Hou et al., 2009), including fatty acids and lipid-derived messengers (Clarke et al., 2002;

Correspondence to Toshinori Hoshi: hoshi@hoshi.org

Abbreviations used in this paper: 17OH DHA, 17-hydroxy docosahexaenoic acid; AA, arachidonic acid; ALA, α-linolenic acid; DHA, docosahexaenoic acid; DHA EE, DHA ethyl ester; dSlo1, *Drosophila melanogaster* Slo1; EPA, eicosapentaenoic acid; hSlo1, human Slo1; Slo1 BK, large-conductance Ca^{2+}- and voltage-gated K^+; VSD, voltage-sensor domain.

The Rockefeller University Press $30.00
J. Gen. Physiol. Vol. 142 No. 5 507–522
www.jgp.org/cgi/doi/10.1085/jgp.201311061

Sun et al., 2007; Vaithianathan et al., 2008; Lai et al., 2009; Wang et al., 2011). Recently, we showed that DHA applied to either side of the membrane potently activates vascular BK channels made of pore-forming Slo1 and auxiliary β1 or β4 subunits (Hoshi et al., 2013c). When examined in inside-out membrane patches, its EC_{50} is estimated to be ∼500 nM, and the stimulatory effect has a fast onset and is reversible on wash-out (Hoshi et al., 2013c). This action on the Slo1 BK channel underlies the acute hypotensive effect of DHA observed when it is injected into anesthetized mice because the effect is absent in mice with the Slo1 gene disrupted (Hoshi et al., 2013c). Unlike DHA, its derivatives, 17-hydroxy DHA (17OH DHA) with a hydroxyl moiety in the tail group and DHA ethyl ester (DHA EE) with an ethyl ester moiety in the head group, are without effect on Slo1 BK channels (Hoshi et al., 2013c). The stimulatory effect of DHA is particularly noticeable when the pore-forming Slo1 subunit is coexpressed with the auxiliary subunit β1, as found in vascular BK channel complexes (Knaus et al., 1994; Wallner et al., 1995), or with β4, as frequently found in neurons (Brenner et al., 2000a; Meera et al., 2000), leading to an increase in macroscopic currents by up to ∼20-fold at some voltages (Hoshi et al., 2013b). When DHA is applied to Slo1 BK channels without heterologously expressed auxiliary subunits, a small current-enhancing effect of DHA is observed, strongly indicating that the presence of β1 or β4 potentiates the functional consequence of DHA binding to the Slo1 subunit (Hoshi et al., 2013b).

In this study, we sought to reveal the biophysical mechanism of the effect of DHA on the Slo1 channel and determine the molecular elements within Slo1 critical for the stimulatory effect. Prompted by the finding that DHA at a functionally saturating concentration for human Slo1 (hSlo1) is without effect on *Drosophila melanogaster* Slo1 (dSlo1), we used chimeric constructs encompassing dSlo1 and hSlo1 channels. Our electrophysiological measurements show that a single residue near the cytoplasmic end of S6 plays a critical role in the differential responses of hSlo1 and dSlo1 channels to select free long-chain omega-3 fatty acids.

MATERIALS AND METHODS

Channel expression

Human embryonic kidney tsA cells were transiently transfected with plasmid DNAs encoding Slo1 channels and monomeric enhanced green fluorescent protein (GFP) as a transfection marker using FuGene6 (Roche). The cells were grown in Dulbecco's modified Eagle's medium, 10% FBS, 1% penicillin/streptomycin at

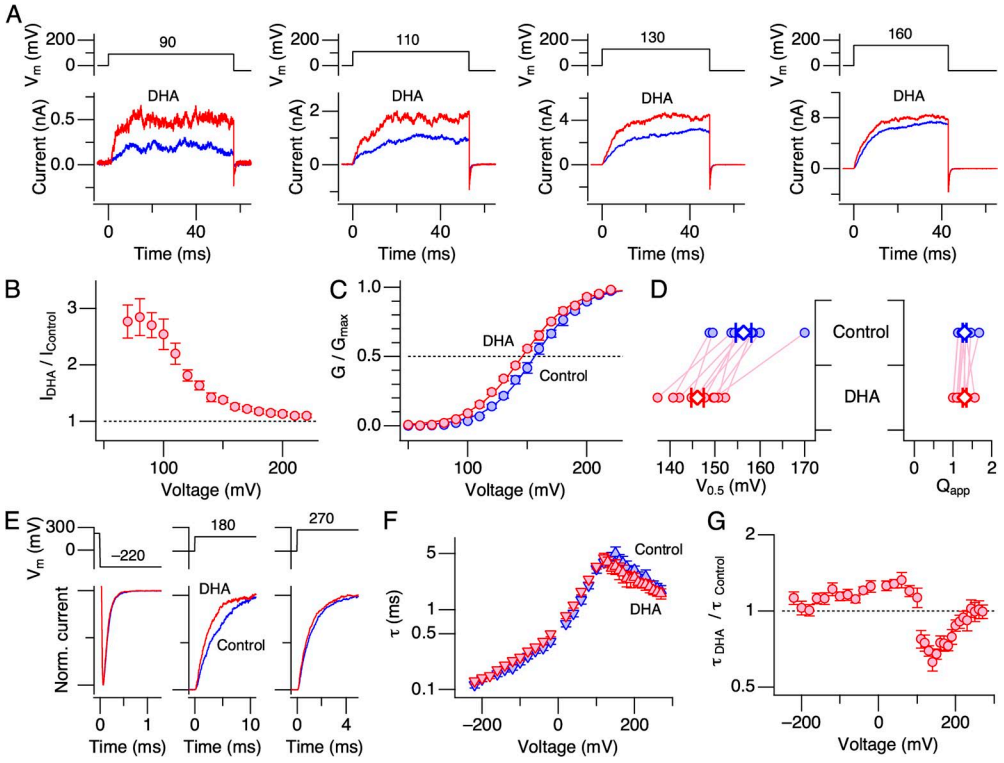

Figure 1. DHA increases currents through hSlo1 channels in the absence of intracellular Ca^{2+}. (A) Representative hSlo1 currents before (blue) and after (red) the application of DHA to the intracellular side. (B) Fractional increases in peak outward currents at different voltages by DHA. $n = 11$. (C) Mean G-V curves before (blue) and after (red) the application of DHA. The smooth curves are Boltzmann fits to the datasets. The $V_{0.5}$ and Q_{app} values for the control group are 156.2 ± 0.78 mV and 1.27 ± 0.05, and for the DHA group, they are 145.9 ± 0.86 mV and 1.18 ± 0.04, respectively. $n = 11$. (D) Changes in $V_{0.5}$ and Q_{app} by DHA in the individual experiments analyzed. The control values are shown in blue, and the values after the addition of DHA are shown in red. The mean values are shown using large diamonds. The $V_{0.5}$ values are statistically different before and after DHA application ($P < 0.001$), but the Q_{app} values are indistinguishable ($P = 0.08$). (E) Comparison of the current kinetics at three different voltages before (blue) and after (red) the application of DHA in a representative patch. The currents were scaled to facilitate comparison. (F) Voltage dependence of time constant of current relaxation before (blue) and after (red) the application of DHA. $n = 6$–9, depending on the voltage. (G) Fractional changes in time constant of current relaxation by DHA at different voltages. $n = 6$–9, depending on the voltage. DHA was applied at 3 μM.

37°C, and 5% CO_2, and used in experiments typically 1–3 d after transfection. The amino acid residue numbering of hSlo1 described here is based on GenBank accession number AAB65837, and that of dSlo1 is based on RefSeq accession number NP_001014653. In some experiments, the plasmids coding for hSlo1 β1 (hβ1; RefSeq accession no. NP_004128) fused with enhanced GFP at the C terminus or hSlo1 β4 (hβ4; GenBank accession no. AAF69805) fused with GFP at the C terminus (Hoshi et al., 2013b) were cotransfected with the hSlo1 plasmid (weight ratio of 1:1) as described previously (Hoshi et al., 2013b). Functional assembly of hSlo1 and hβ subunits in each patch was confirmed as described previously (Hoshi et al., 2013b). The presence of the C-terminal GFP tag does not alter the response of the hSlo1+hβ1 or hSlo1+hβ4 complex to DHA (Hoshi et al., 2013c).

Mutagenesis

Single–amino acid mutations were introduced into hSlo1 (pCI-neo) and dSlo1 (pRc/CMV) using a commercially available kit (QuickChange; Agilent Technologies), and the sequences were verified. The chimeric constructs were generated using the method of Yon and Fried (1989).

Data acquisition and analysis

The experiments were performed at room temperature as described previously (Horrigan et al., 2005). For the pharmacological experiments described here, only those results obtained from membrane patches that formed high resistance seals very quickly, less than several seconds, without excess negative pressure were used. The membrane patches formed in this manner were devoid of much cytoplasmic material, based on visual inspection with bright field and/or fluorescent microscopy, and the channels contained therein responded quickly to DHA and other agents (Hoshi et al., 2013b). Large omega-shaped membrane patches, although they produced large ionic currents, were not used for the pharmacological experiments described. Macroscopic currents were recorded with pipettes with initial resistances of 0.5–2 MΩ, and 60–70% of the initial resistance was electronically compensated. Unless otherwise noted, capacitive and leak currents have been subtracted from the results shown. For single-channel measurements, the pipette diameter was adjusted to obtain desired numbers of channels. The output signal of the amplifier (Axopatch 200A or 200B; Molecular Devices) was filtered through the amplifier's built-in 10-kHz filter and digitized.

The results were analyzed using IgorPro (WaveMetrics) as described previously (Horrigan et al., 2005). Normalized macroscopic G-V curves were estimated from extrapolated instantaneous tail current sizes and characterized by a Boltzmann function,

$$\frac{G(V_m)}{G_{max}} = \frac{I(0,V_m)}{I_{max}(0)} \frac{1}{1+e^{-(V_m-V_{0.5})\frac{(Q_{app}F)}{RT}}},$$

where $G(V_m)/G_{max}$ represents the normalized conductance at the membrane potential V_m; $I(0, V_m)/I_{max}$ (0) is the normalized extrapolated instantaneous tail current size after a pulse to V_m; and F, R, and T have their usual meanings. The half-activation voltage ($V_{0.5}$) and the number of apparent equivalent charges (Q_{app}) were used as data description parameters. Macroscopic ionic current kinetics was fitted with a single exponential. The time constant values were estimated from currents elicited by depolarization (triangles in the figures) and from tail currents (inverse triangles in the figures).

Single-channel ionic currents were recorded through the 500-MΩ feedback resistor of the amplifier, filtered through the built-in 10-kHz filter, and digitized at 83 or 100 kHz. Single-channel open probability (P_o) was inferred by generating all-point amplitude histograms, and the number of channels present in each patch was estimated from the macroscopic current size at 220 mV (Horrigan et al., 2005). In single-channel experiments with dSlo1, the number of channels present was not estimated. The single-channel open duration analysis was performed as described previously (Avdonin et al., 2003; Horrigan et al., 2005), and no left-censor correction was made.

Solutions and reagents

The extracellular solution contained (mM): 140 KCl, 2 $MgCl_2$, and 10 HEPES, pH 7.2 with *N*-methyl-D-glucamine (NMG). The Ca^{2+}-free internal solution contained (mM): 140 KCl, 11 EGTA, 0.02 18C6TA, and 10 HEPES, pH 7.2 with NMG. Other solutions used are described in the legends to the figures. The fatty acid solutions were prepared immediately before measurements as described previously (Hoshi et al., 2013b,c). DHA was applied after the ionic currents stabilized after patch excision. This was particularly important for the experiments using dSlo1 channels, which often showed noticeable "run-up." Unless otherwise noted, DHA was typically applied at 3 µM because this concentration represents a nearly saturating concentration to stimulate BK channels (Hoshi et al., 2013c; also see Fig. S1). DHA, α-linolenic acid (ALA), and arachidonic acid (AA) were obtained from Sigma-Aldrich. 17OH DHA, DHA EE, and EPA were purchased from Cayman Chemical Company.

Statistical evaluations

Equation parameters are presented as mean ± 95% confidence interval as implemented in IgorPro. Statistical results are presented in the text as mean ± SEM (n), where n is the number of independent measurements. The error bars in the figures represent SEM.

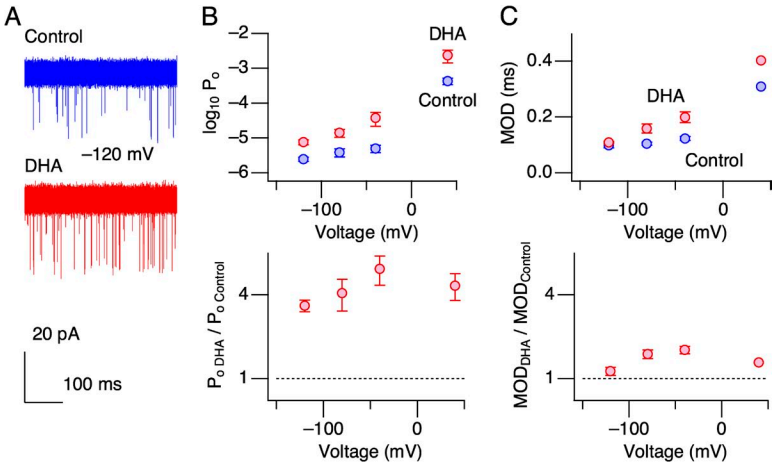

Figure 2. Single-channel openings at negative voltages in the absence of intracellular Ca^{2+}. (A) Representative hSlo1 openings at −120 mV before (top) and after (bottom) the addition of DHA. This patch contained ∼140 channels, and 20 40-ms segments are shown superimposed in each condition. (B) P_o before (blue) and after (red) DHA addition (top) and fractional increases in P_o by DHA (bottom) at different voltages. n = 6–9, depending on the voltage. (C) Mean open durations (MODs) before (blue) and after (red) DHA application (top) and fractional increases in MODs by DHA at different voltages (bottom). n = 5. DHA was applied at 3 µM.

Statistical comparisons of the results were performed using the two-sided Mann-Whitney or Wilcoxon test, with the significance level of 0.05 in IgorPro as appropriate. For comparisons of three or more groups, the significance level was corrected using the Bonferroni method.

Online supplemental material

Fig. S1 illustrates that increasing the concentration of DHA from 3 to 10 µM does not lead to any additional increase in currents through hSlo1 channels; 3 µM DHA is a saturating concentration. Fig. S1 also shows that the stimulatory effect of DHA is reversible. Fig. S2 presents G-V curves of hSlo1–dSlo1 chimeric channels in the absence of Ca^{2+} and DHA. Fig. S3 shows single-channel openings from hSlo1(1:327)–dSlo1(342:1164) where the entire C-terminal area of hSlo1 is replaced with that of dSlo1. DHA increases open probability in this chimeric channel, illustrating that the S0–S6 segments of hSlo1 possess the molecular elements required for the stimulatory action of DHA. Fig. S4 depicts the essential characteristics of the stimulatory action of 3 µM DHA in the absence of Ca^{2+} in hSlo1+hβ1; DHA increases currents by up to ∼20-fold (A and B) and shifts G-V by approximately −60 mV. Fig. S5 compares the effects of DHA on the kinetics of ionic current relaxation in hSlo1+hβ1 and hSlo1 Y318S+hβ1. The online supplemental material is available at http://www.jgp.org/cgi/content/full/jgp.201311061/DC1.

RESULTS

Effects of DHA on hSlo1 channels without auxiliary subunits

3 µM DHA applied to the intracellular side in the virtual absence of Ca^{2+} increased macroscopic K^+ currents through hSlo1 channels in the absence of heterologously expressed auxiliary subunits (herein referred to as hSlo1 channels; Fig. 1). As found with Slo1+β1 channels (Hoshi et al., 2013c), 3 µM DHA is a saturating concentration in increasing Slo1 currents; 10 µM caused no further increase (Fig. S1 A). Greater fractional increases were observed at less depolarized voltages (Fig. 1, A and B), and the increase in macroscopic current peaked at ∼2.5-fold (Fig. 1 B). After DHA application, the macroscopic G-V curve shifted by −10.3 ± 1.5 mV (11) (Fig. 1, C and D; $P < 0.0001$) without a significant change in its steepness (Q_{app} after DHA/Q_{app} before = Q_{app} ratio = 0.94 ± 0.03 [11]; Fig. 1 D; $P = 0.08$). The shift in G-V $V_{0.5}$ ($\Delta V_{0.5}$) in hSlo1 channels was modest and much smaller than that previously observed in hSlo1+hβ1 channels, approximately −58 mV (Hoshi et al., 2013c), but the effect was reversible (Fig. S1 B). The application of DHA also modestly altered the kinetics of ionic currents. Although the kinetics at extreme negative and positive voltages remained largely unaltered, the time course of current relaxation was noticeably faster at intermediate voltages (e.g., 160 mV, where G/G_{max} is ∼0.5) after DHA application (Fig. 1, E–G).

In hSlo1+hβ1 channels, we reported that activation of the voltage-sensor domain (VSD) was not required for the stimulatory effect of DHA because it increased the channel open probability (P_o) robustly (>20-fold) at very negative voltages in the absence of Ca^{2+} (Hoshi et al., 2013c). In hSlo1 channels, we found a similar but smaller (approximately fourfold) increase in P_o at negative voltages without Ca^{2+} (Fig. 2, A and B). The mean open durations remained relatively unaltered (1.3- to 1.6-fold increases; Fig. 2 B, bottom) after DHA application. Because P_o at these negative voltages is determined primarily by a single closed–open transition of the ion conduction gate (Horrigan et al., 1999), DHA most probably increases the rate constant of gate opening by 3- to 2.5-fold.

We also showed earlier that the effect of DHA on hSlo1+hβ1 channels was maintained at $[Ca^{2+}]_i \geq 100$ µM (Hoshi et al., 2013c), where the Ca^{2+} sensors are largely saturated with Ca^{2+} (summarized in Hoshi et al., 2013a). In hSlo1 channels, DHA was also effective at 300 µM $[Ca^{2+}]_i$, increasing currents by up to fourfold (Fig. 3, A–C) and causing a small but noticeable left-shift in G-V (Fig. 3 D).

The electrophysiological effects of DHA on hSlo1 are thus similar to those observed on hSlo1+β1. In both channel types, DHA promotes opening of the ion conduction gate without any need for activation of the VSDs or the Ca^{2+} sensors. However, the effect of DHA on the ion conduction gate is clearly much greater in

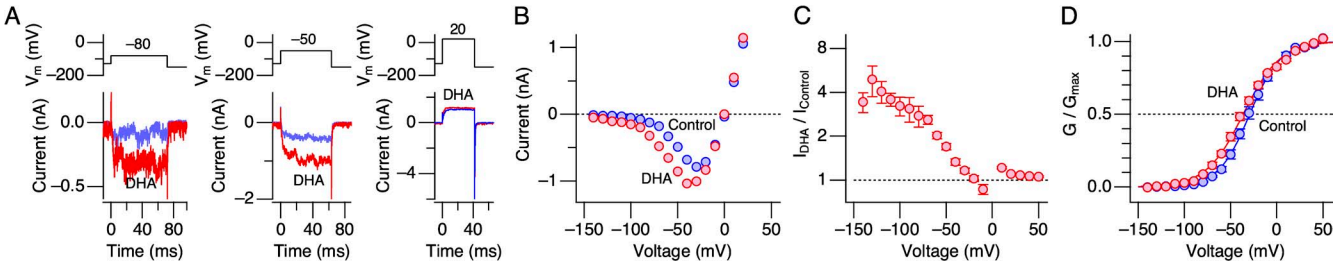

Figure 3. DHA increases currents through hSlo1 channels in the presence of 300 µM of intracellular Ca^{2+}. (A) Representative currents before (blue) and after (red) the application of DHA. No leak current subtraction. (B) Representative I-V curves before (blue) and after (red) the application of DHA. (C) Fractional increases in peak currents at different voltages by DHA. $n = 6$. (D) G-V curves before (blue) and after (red) the application of DHA. The smooth curves are Boltzmann fits to the results. The $V_{0.5}$ and Q_{app} values for the control condition are −29.3 ± 0.92 mV and 1.48 ± 0.07, and for the results obtained with DHA, the values are −36.4 ± 1.7 mV and 1.25 ± 0.09, respectively. $n = 6$. The $V_{0.5}$ values are statistically different ($P = 0.031$), but the Q_{app} values are indistinguishable ($P = 0.063$). DHA was applied at 3 µM.

the hSlo1+β1 channel than in the hSlo1 channel. The results are collectively consistent with the idea that the functional consequence of the interaction of DHA with the Slo1 protein is amplified by the presence of β1 (Hoshi et al., 2013c).

DHA is without effect on dSlo1 channels

In humans, DHA is an essential fatty acid and plays critical roles in various organs, especially in the brain (Lauritzen et al., 2001; Horrocks and Farooqui, 2004). In contrast, the fruit fly *Drosophila* normally lacks DHA in the body (Shen et al., 2010). As an initial step toward identification of the molecular elements within the hSlo1 channel critical for the stimulatory effect of DHA, we examined how DHA affected hSlo1 and dSlo1 channels. Currents through dSlo1 channels were very slow to activate and required much greater and longer depolarization than that needed for hSlo1 channels; in the absence of Ca^{2+}, the mean $V_{0.5}$ value for dSlo1 was 245.0 ± 1.0 mV (5) compared with the mean $V_{0.5}$ value of 156.2 ± 0.78 mV (11) for hSlo1 (Fig. 4, A and B). The slow kinetics and the right-shifted voltage dependence of steady-state activation made it impractical to systematically study the effects of DHA on dSlo1 G-V as performed with hSlo1 (see Fig. 1); the integrity of high resistance seals was easily compromised by long and large voltage pulses. Thus, we opted to examine the outward currents through dSlo1 only at 140, 170, and 200 mV, which correspond roughly to G/G_{max} of 0.02, 0.06, and 0.15 based on the results shown in Fig. 4 B. In hSlo1 channels, at the equivalent G/G_{max} voltages, DHA has clear current-enhancing effects (see Fig. 1). The application of 3 µM DHA to dSlo1 channels

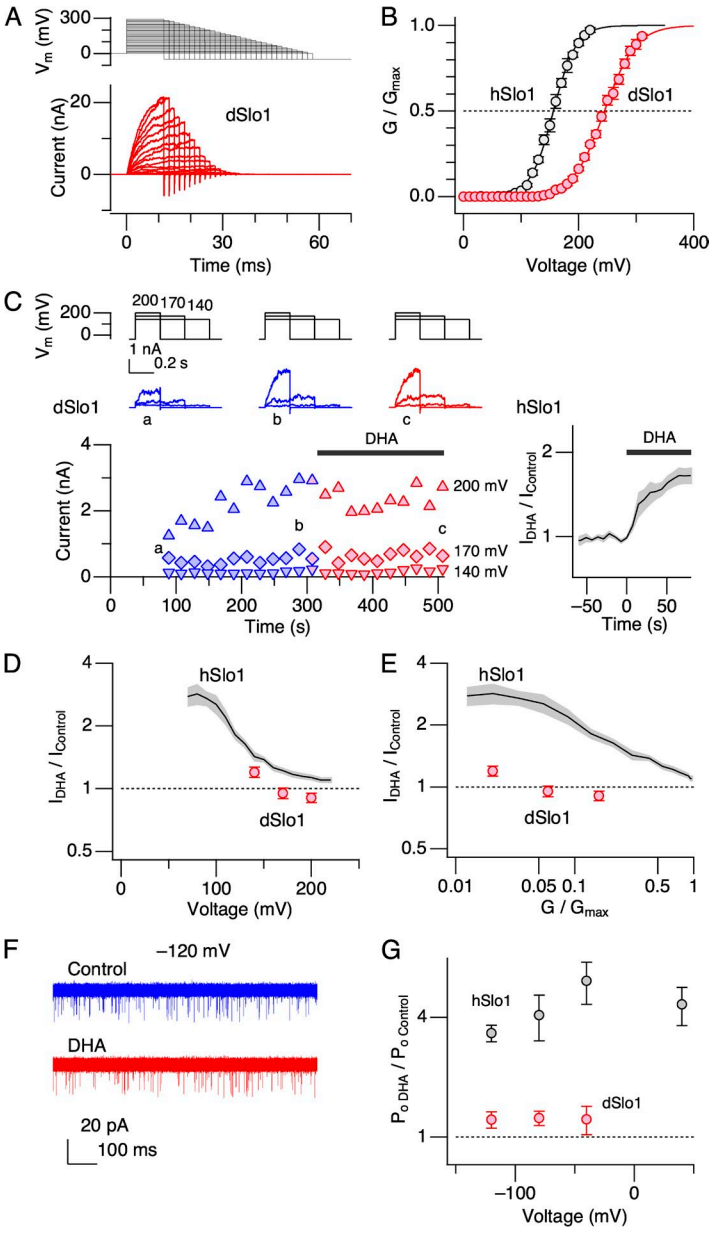

Figure 4. Currents through dSlo1 channels do not respond to DHA. (A) Currents through dSlo1 channels in a patch (bottom) elicited by the voltage pulses indicated (top). (B) G-V curves for dSlo1 (red) and hSlo1 (black). The smooth curves represent Boltzmann fits to the datasets. The $V_{0.5}$ and Q_{app} values for dSlo1 are 245.0 ± 1.0 mV and 0.92 ± 0.03 (n = 5), and for hSlo1, the values are 156.2 ± 0.78 mV and 1.27 ± 0.05 (n = 11). (C) Representative currents through dSlo1 elicited by pulses to 140, 170, and 200 mV (top left) and the peak outward current sizes as a function of time (bottom left). DHA was present during the time indicated by the gray horizontal bar. The patch was excised at t = 0. The graph on the right shows the kinetics of current increase in hSlo1 by DHA for comparison (n = 15). (D) Fractional increases in peak outward currents through dSlo1 as a function of voltage (red; n = 17–22, depending on the voltage). The results obtained for hSlo1 are shown using the black curve and the surrounding gray area (mean ± SEM). (E) Fractional increases in peak outward currents through dSlo1 as a function of G/G_{max}. The results shown in D are transformed using the G-V curves in B. (F) Representative openings of dSlo1 at −120 mV before (top) and after (bottom) the addition of DHA. For each group, 25 1-s segments are superimposed and displayed. (G) Estimated fractional increases in P_o by DHA at different voltages. n = 7 at each voltage. The currents were recorded in the absence of Ca^{2+}. DHA was applied at 3 µM.

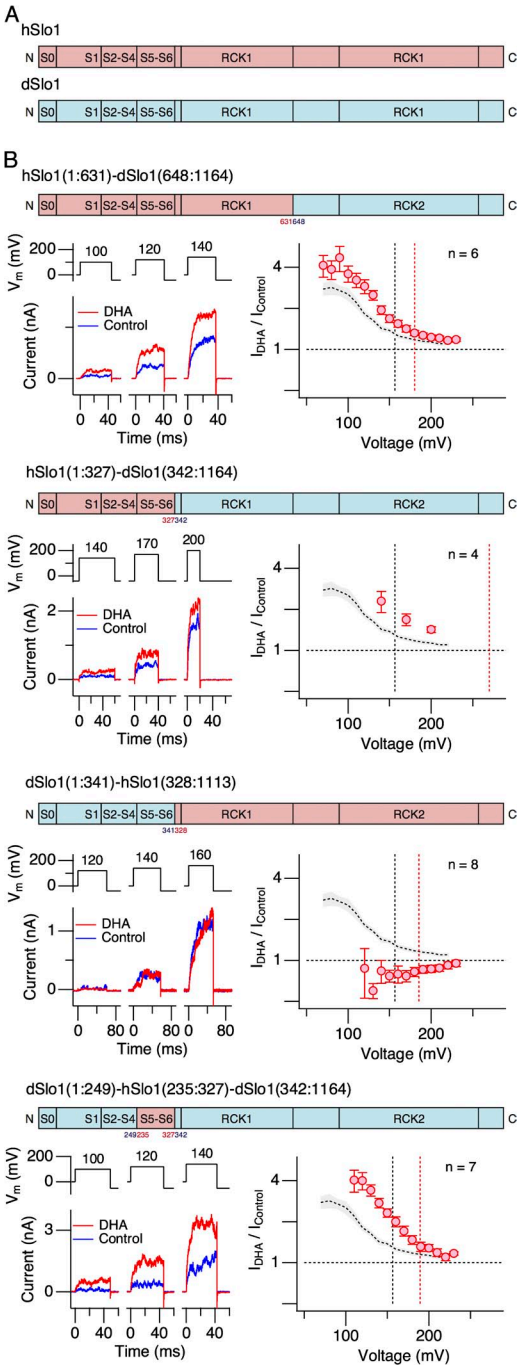

Figure 5. Currents through human–*Drosophila* chimeric Slo1 channels. (A) Schematic organizational diagrams of hSlo1 (pink) and dSlo1 (light blue). (B) Currents through four different human–*Drosophila* chimeric Slo1 channels. For each construct, a schematic organizational diagram, sample currents at three different voltages before (blue) and after (red) the application of 3 µM DHA, and fractional increases in peak outward currents at different voltages, are presented. In the organization diagrams, the pink and light blue regions represent hSlo1 and dSlo1, respectively. In each $I_{DHA}/I_{Control}$ graph, the red dashed vertical line indicates the G-V $V_{0.5}$ value for the chimeric channel, the black dashed line shows the $V_{0.5}$ value of hSlo1, and the dashed gray curve represents the results obtained for hSlo1 (mean ± SEM) for comparison.

produced virtually no change in currents at these three voltages for up to 200 s or more (Fig. 4 C, left). In comparison, DHA increases currents through hSlo1 within 50 s of application (Fig. 4 C, right). The mean fractional change in the dSlo1 current size was at most only 1.19 ± 0.07 (17) (at 140 mV; Fig. 4 D). When the fractional changes in dSlo1 and hSlo1 currents were plotted against their estimated G/G_{max} values, the ineffectiveness of DHA on dSlo1 was made even more evident (Fig. 4 E). Additionally, single-channel measurements failed to detect any significant effect of 3 µM DHA at negative voltages where the VSDs are expected to be at rest (P = 0.94, 0.22, and 0.16 at −40, −80, and −120 mV, respectively; Fig. 4, F and G), and the relative changes in P_o in dSlo1 by 3 µM DHA were different from those found in hSlo1 at the same voltages (P = 0.001, 0.0003, and 0.0006 at −40, −80, and −120 mV, respectively). *Drosophila* possesses cytoplasmic auxiliary subunits that are structurally distinct from vertebrate β subunits (Schopperle et al., 1998); therefore, we did not test if the *Drosophila* auxiliary subunits alter the response to DHA.

The contrasting effects of DHA on hSlo1 and dSlo1 prompted us to generate chimeric constructs encompassing the two Slo1 channel types, and some of the chimeric channels examined are shown in Fig. 5. Because many of the chimeric channels did not express well and/or had right-shifted voltage dependence (Fig. S2), their G-V parameters were difficult to estimate accurately. Thus, we used fractional changes in peak outward current as the dependent variable. DHA noticeably increased currents through hSlo1(1:631)–dSlo1(648:1164), in which essentially the RCK2 segment of hSlo1 (residues 631 through 1113) is replaced with that of dSlo1 (residues 648 through 1164; Fig. 5 B, top). Substitution of the entire C-terminal cytoplasmic area of hSlo1 containing both the RCK1 and RCK2 domains with the corresponding area of dSlo1 (hSlo1(1:327)–dSlo1(342:1164)) drastically decreased the expression efficacy and also shifted the voltage dependence of activation to the positive direction ($V_{0.5}$ = 270.8 ± 2.6 mV [4]); however, the currents recorded were enhanced by DHA (Fig. 5 B, second from top, and Fig. S3). In contrast, substitution of the S0–S6 segments of hSlo1 with the corresponding segments of dSlo1 (dSlo1(1:341)–hSlo1(328:1113)) obliterated the stimulatory effect of DHA (Fig. 5 B, third from top), potentially signifying the importance of the transmembrane segments. Importantly, DHA clearly enhanced currents through dSlo1(1:249)–hSlo1(235:327)–dSlo1(342:1164), in which the S5-P-S6 segments of dSlo1 are replaced with those of hSlo1 (Fig. 5 B, bottom). The fractional increases in peak outward currents of this chimeric construct resembled those from hSlo1 channels (Fig. 5 B, bottom right).

The human-to-*Drosophila* mutation Y318S

The results from the hSlo1–dSlo1 chimeric constructs suggested the importance of the pore domain encompassing

the S5, P, and S6 segments in mediating the current-enhancing effect of DHA observed in hSlo1. To further delineate the structural elements required for the DHA action, we introduced human-to-*Drosophila* point mutations in the pore (S5-P-S6) domain of the hSlo1 channel. The hSlo1 channel was used as the "background" channel because it expressed better than dSlo1 and its voltage dependence was much more amenable for electrophysiological measurements. The extracellular-facing S5-P linker segment, which is not well conserved among Slo1 channels from different species (e.g., *Drosophila* vs. *Periplaneta americana*), was not included in this mutagenesis strategy. Because the stimulatory effect of DHA on hSlo1 channels without any auxiliary subunit is small and difficult to study, producing only a $\Delta V_{0.5}$ of about −10 mV (Fig. 1), we initially compared the effects of DHA on the hSlo1 channels with human-to-*Drosophila* mutations when coexpressed with hβ1. In wild-type hSlo1+hβ1 channels, DHA causes a readily discernible shift in G-V, of approximately −60 mV (Fig. S4). The strategy here was to identify those human-to-*Drosophila* mutations in hSlo1 that altered $\Delta V_{0.5}$ by DHA when coexpressed with β1 and then to test the Slo1 mutant identified alone without β1. The *Drosophila*-to-human point mutations in hSlo1 effected a variety of changes to hSlo1+β1 (Figs. 6–8 and Table 1). Some of the mutations shifted G-V to the negative direction (V236A in S5 [Fig. 6, top] and L280F in P [Fig. 7, top]), whereas others shifted G-V to the positive direction. In particular, the mutations F252I in the S5 segment (Fig. 6) and M282I in the P segment (Fig. 7) markedly

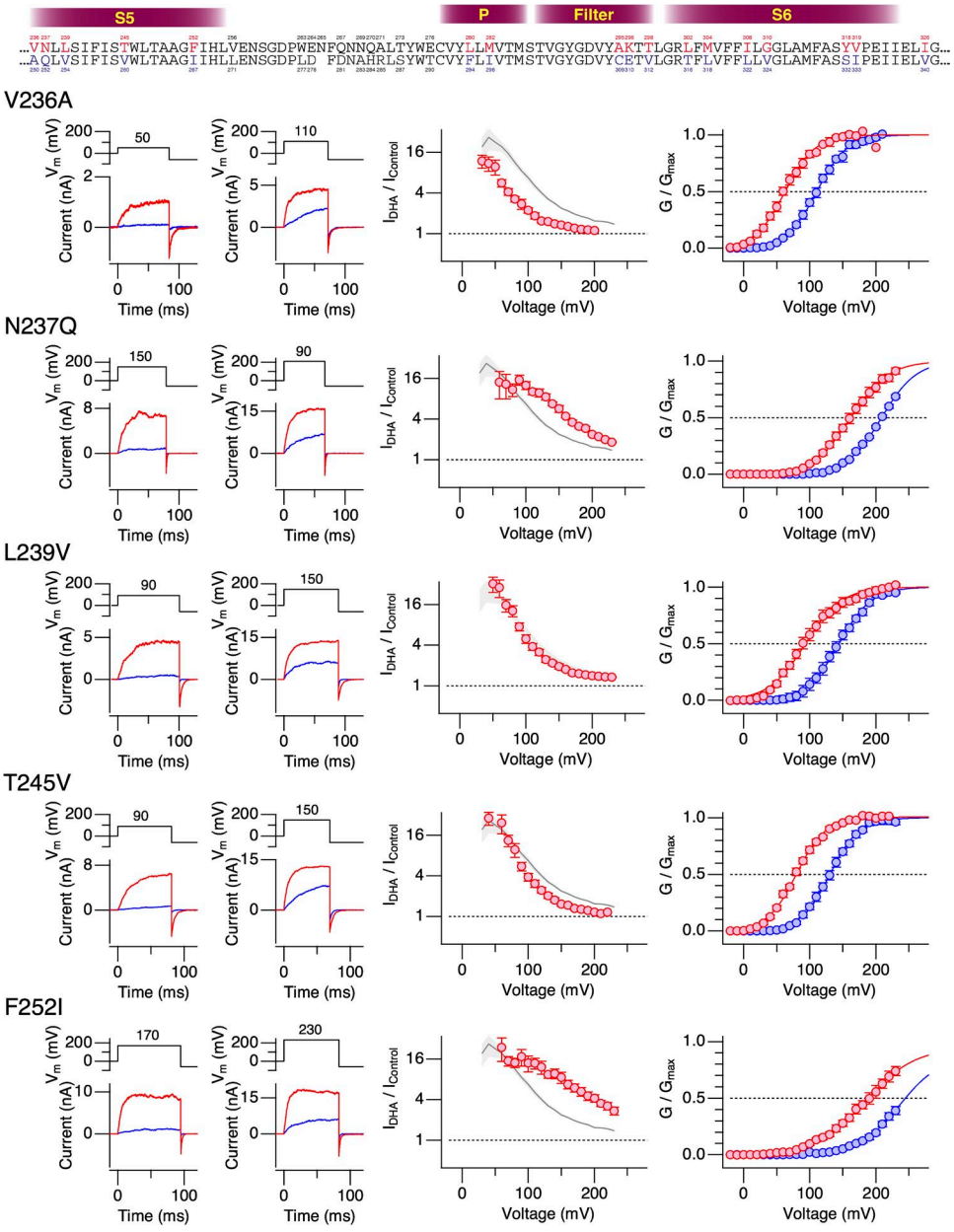

Figure 6. Changes in properties of hSlo1+hβ1 complexes bearing human-to-*Drosophila* mutations in the S5 segment by 3 μM DHA in the absence of intracellular Ca^{2+}. For each mutant, sample currents before (blue) and after (red) the application of DHA at two different voltages where the control G/G_{max} values are ∼0.1 and ∼0.5, fractional increases in peak outward currents at different voltages, and G-V curves before (blue) and after (red) the application of DHA are depicted. The smooth curves are Boltzmann fits to the datasets before and after the application of DHA (see Table 1 for the parameter values).

moved $V_{0.5}$ to ~250 mV, similar to the mean $V_{0.5}$ value of dSlo1. In these extreme right-shifted mutants, accurate determinations of the G-V parameters were difficult. The *Drosophila*-to-human mutations I308L and G310V in S6 individually rendered the resulting channels electrophysiologically nonfunctional. However, the double mutant hSlo1 I308L:G310V was functional. In almost every mutant channel complex examined, DHA increased currents and caused a clear shift in $V_{0.5}$ to the negative direction (Figs. 6–9). The only exception was hSlo1 Y318S+hβ1. In this channel complex bearing a mutation toward the C-terminal end of S6, DHA caused negligible changes in current size and $V_{0.5}$ (Figs. 8 and 9). DHA markedly accelerates the activation kinetics and slightly slows the deactivation kinetics in wild-type Slo1+hβ1 (Hoshi et al., 2013c). In contrast, DHA only moderately accelerated the current relaxation kinetics at all voltages in hSlo1 Y318S+hβ1 (Fig. S5). We verified that hSlo1 Y318S functionally assembles with hβ1 by confirming the characteristically slower activation and deactivation when compared with hSlo1 Y318S alone (Fig. 10). Furthermore, the voltage dependence of activation of hSlo1 Y318S+hβ1 at a wide range of $[Ca^{2+}]_i$ without DHA closely resembled that of wild-type hSlo1+hβ1 (Fig. 10 B).

Even without coexpression of β1, 3 µM DHA caused no measurable change in peak outward current size, G-V, or kinetics in hSlo1 Y318S (Fig. 11, A–F). The application of a greater concentration of DHA, 10 µM, also failed to increase currents through hSlo1 Y318S and, in fact, often decreased currents (Fig. 11), potentially suggesting that

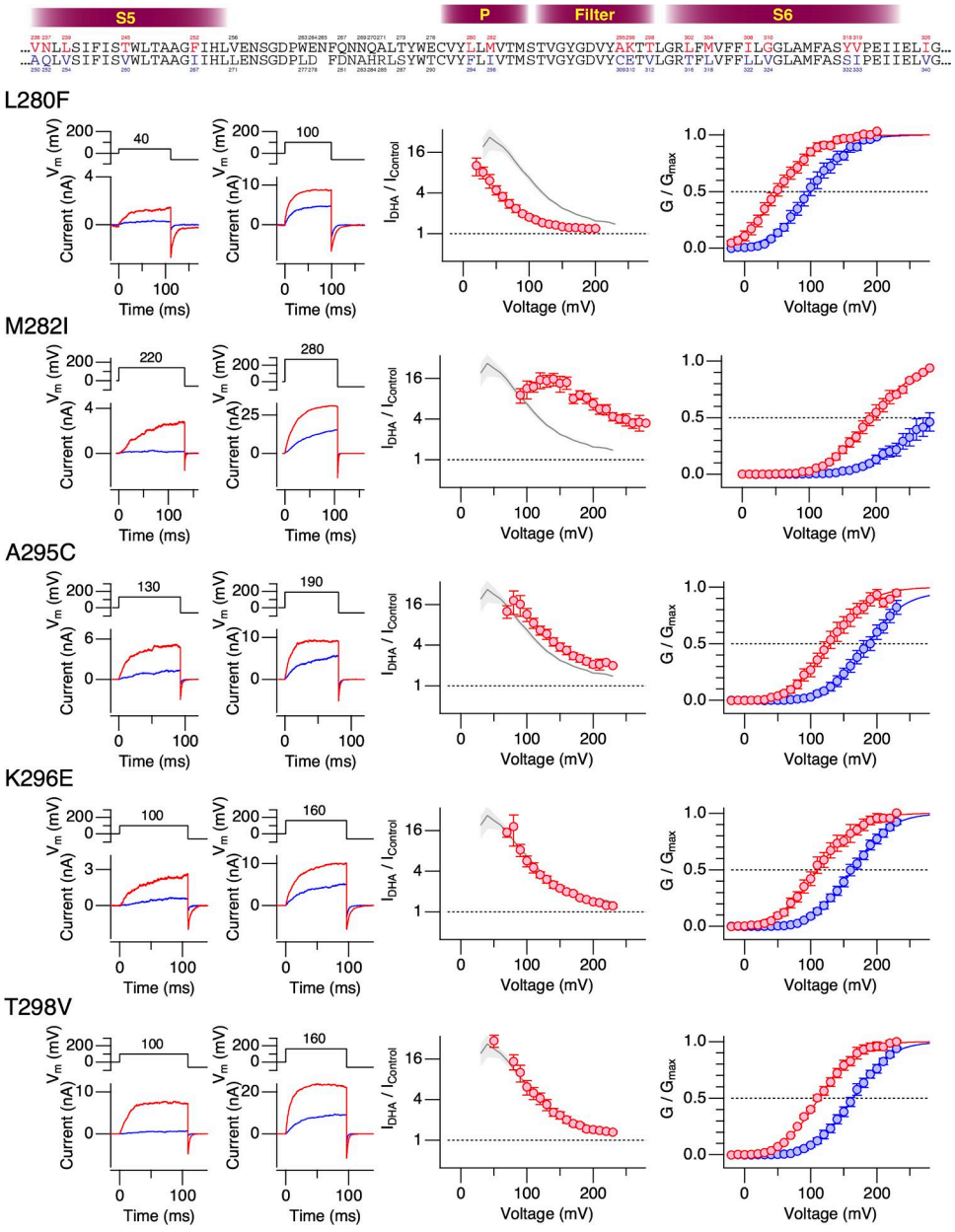

Figure 7. Changes in properties of hSlo1+hβ1 complexes bearing human-to-*Drosophila* mutations in the P/filter segment by 3 µM DHA in the absence of intracellular Ca^{2+}. See Fig. 6 legend for details.

DHA may exert multiple effects on the hSlo1 channel depending on the concentration.

We showed previously that DHA markedly increases currents through vascular hSlo1+hβ1 channels as well as through predominantly neuronal hSlo1+hβ4 channels, causing a $\Delta V_{0.5}$ of approximately −60 mV (Hoshi et al., 2013b). The human-to-*Drosophila* mutation Y318S virtually eliminated the DHA sensitivity in hSlo1 when coexpressed with hβ4 (Fig. 12). We confirmed that hSlo1 Y318S functionally assembled with hβ4 based on the characteristically slow activation kinetics (Fig. 12 A); however, neither the peak outward current size nor the G-V characteristics in hSlo1 Y318S+hβ4 was altered by 3 µM DHA (Fig. 12, B–D).

hSlo1 Y318S+hβ1 channels and other free fatty acids

Currents through hSlo1+hβ1 channels are enhanced by omega-3 and omega-6 fatty acids of different types to various

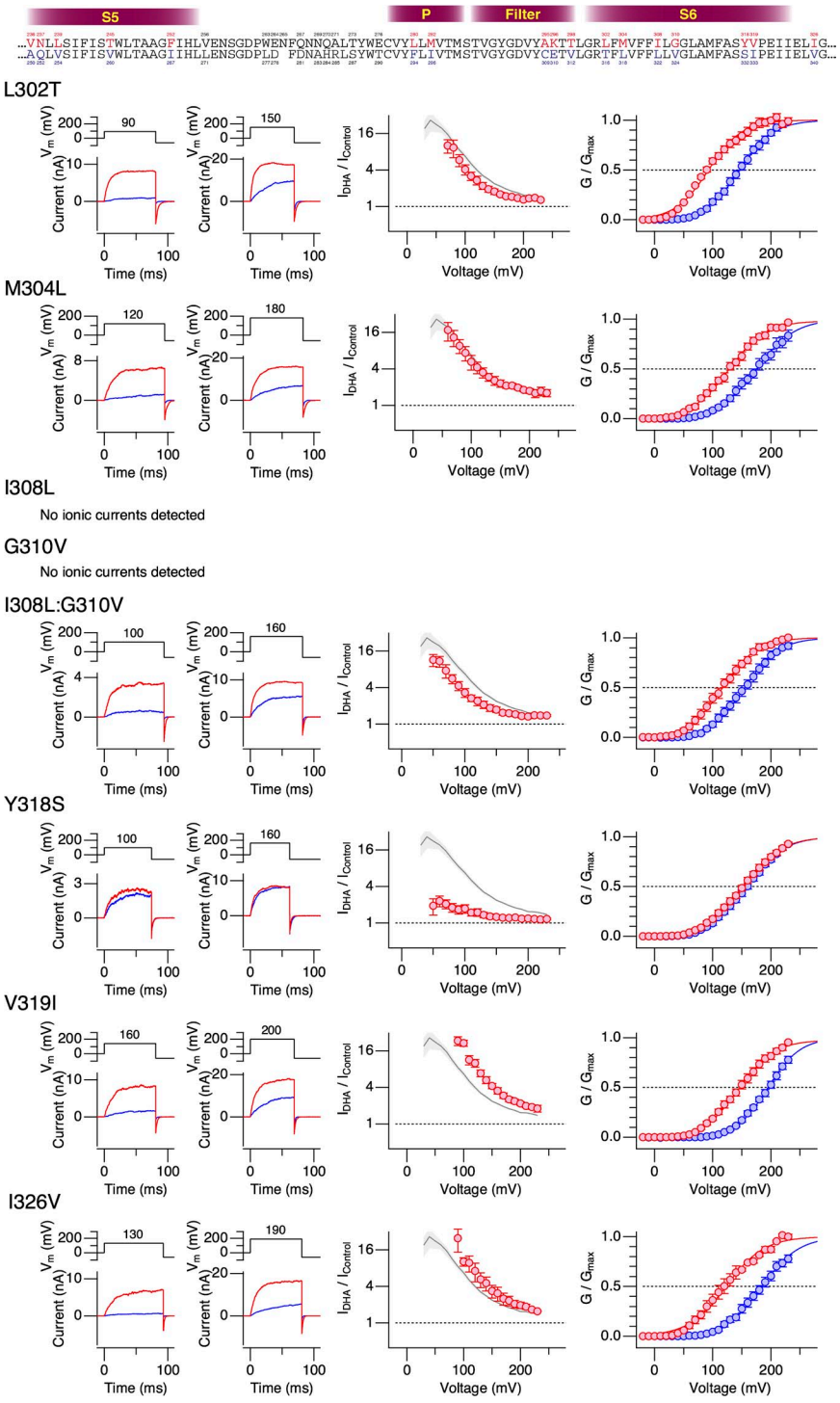

Figure 8. Changes in properties of hSlo1+hβ1 complexes bearing human-to-*Drosophila* mutations in the S6 segment by 3 µM DHA in the absence of intracellular Ca^{2+}. See Fig. 6 legend for details.

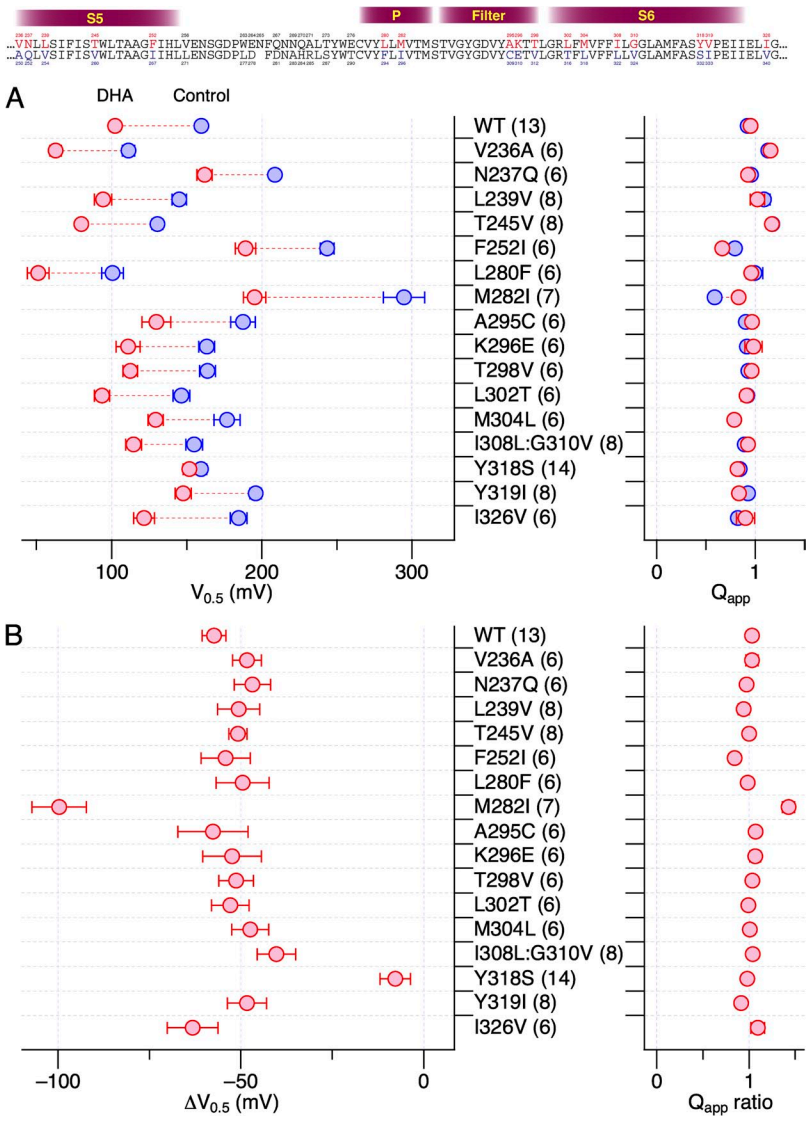

Figure 9. G-V parameters of hSlo1+hβ1 complexes bearing human-to-*Drosophila* mutations in the S5, P/filter, and S6 segments by 3 µM DHA. (A) The results obtained before (blue) and after (red) the addition of DHA are compared. (B) Changes in $V_{0.5}$ and fractional changes in Q_{app} by DHA. When compared with the values in the WT group, only the $\Delta V_{0.5}$ values for Y318S are statistically distinct ($P < 10^{-7}$) after correcting the significance level for 16-way comparisons with the wild-type values. All results were obtained without intracellular Ca^{2+}.

degrees (Hoshi et al., 2013c). Our previous structure–activity experiments suggested the importance of both the polar "head" group and the long hydrophobic "tail" group. DHA EE with an ethyl ester group in the head group is essentially ineffective in modulating in hSlo1+hβ1 channels. DHA with a 22-carbon tail is more effective in shifting $V_{0.5}$ than the shorter omega-3 fatty acids EPA, with a 20-carbon tail, and ALA (18:3(ω-3)), with an 18-carbon tail. The presence of an OH moiety in the tail group in 17OH DHA also greatly impairs the effectiveness. AA (20:4(ω-6)), an omega-6 fatty acid with a 20-carbon chain, is less effective than DHA. We compared the effectiveness of these fatty acids (Fig. 13 A) on hSlo1 Y318S+hβ1 channels by measuring the $\Delta V_{0.5}$ and Q_{app} ratio values. To facilitate comparison, the results obtained with wild-type hSlo1+hβ1 channels (Hoshi et al., 2013b,c) are illustrated with gray bars in Fig. 13 B, and the differences in $\Delta V_{0.5}$ observed between wild-type hSlo1+hβ1 and hSlo1 Y318S+hβ1 channels are summarized in Fig. 13 C. When corrected for multiple comparisons, only the $\Delta V_{0.5}$ values for DHA and EPA are significantly different between wild-type hSlo1+hβ1 and hSlo1 Y318+hβ1 ($P < 10^{-7}$). It is noteworthy that ALA, the shortest omega-3 fatty acid

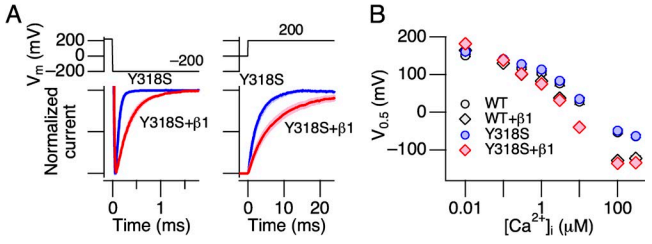

Figure 10. hSlo1 Y318S functionally coassembles with hβ1. (A) Comparison of mean normalized currents at −200 mV (left) and 200 mV (right) from patches taken from cells transfected with hSlo1 Y318S DNA (blue) and those cotransfected with hSlo1 Y318S and hβ1 DNAs together. The line width indicates SEM. n = 6–18. (B) Ca^{2+} dependence of G-V $V_{0.5}$ in wild-type Slo1 alone (WT; black circles), wild-type hSlo1+hβ1 (black diamonds), hSlo1 Y318S alone (blue circles), and hSlo1 Y318S+hβ1 (red diamonds). n = 6–12. The solution with 11 mM EGTA but without any added Ca^{2+} was assumed to have 10 nM of free Ca^{2+}.

tested, and AA, an omega-6 fatty acid, remained equally effective in wild-type hSlo1+hβ1 and hSlo1 Y318S+hβ1 (Fig. 13, B, left, and C). The effect of the mutation Y318S on hSlo1 may be preferential to DHA and EPA, two long-chain omega-3 fatty acids.

The *Drosophila*-to-human mutation S332Y in dSlo1

We introduced the *Drosophila*-to-human mutation S332Y into dSlo1, the converse of the human-to-*Drosophila* mutation hSlo1 Y318S, and examined whether the mutation introduced any noticeable DHA sensitivity to the dSlo1 channel. The voltage dependence of activation of dSlo1 S332Y remained shifted to the positive direction compared with that of hSlo1 (Fig. 14, A and B), and we therefore compared ionic current sizes at three different voltages (Fig. 14 C). DHA did not markedly alter the currents through dSlo1 S332Y (Fig. 14, C and D).

DISCUSSION

Our ionic current measurements presented here show that the mechanism of the action of DHA on the hSlo1 channel without any β subunit, at least qualitatively, resembles that observed in the hSlo1+hβ1 channel (Hoshi

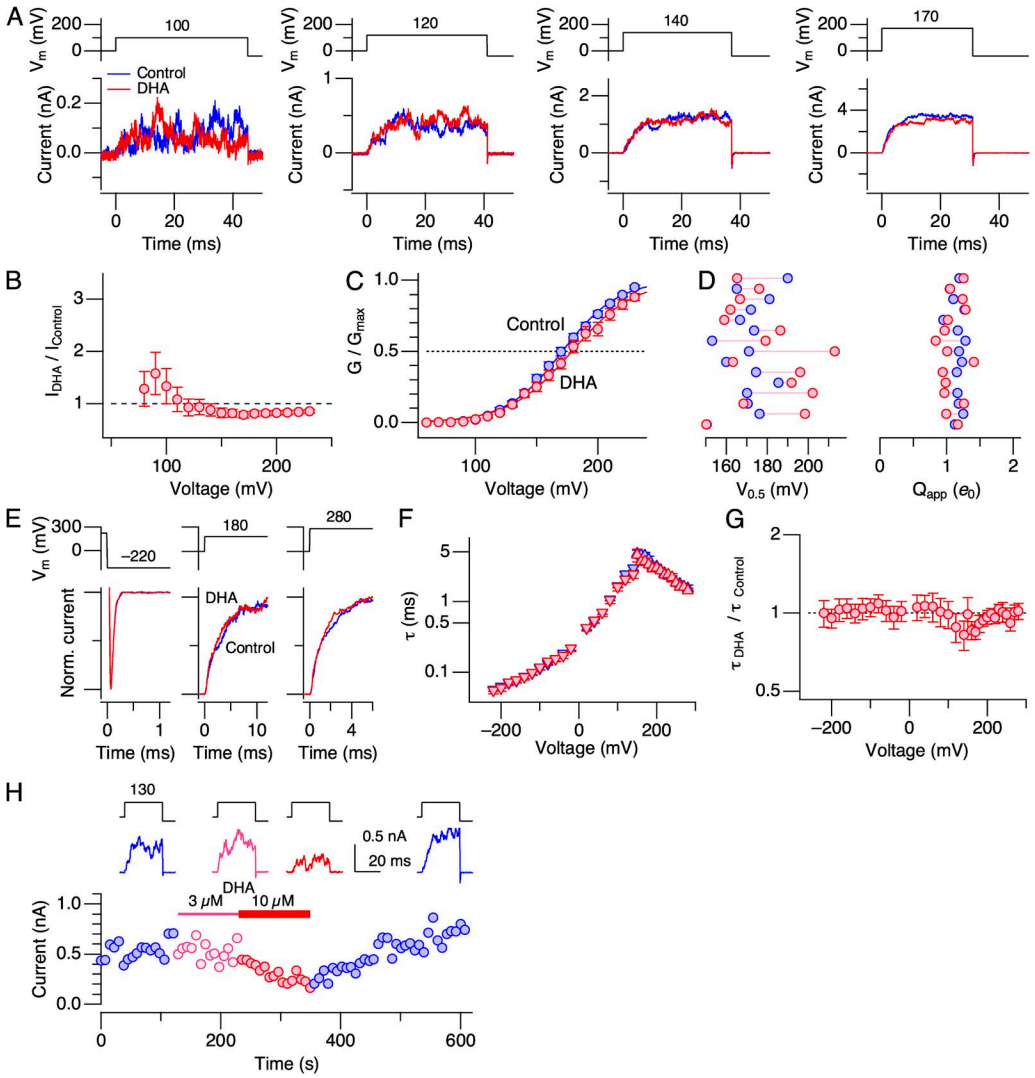

Figure 11. Currents through hSlo1 Y318S are largely unaltered by DHA. (A) Representative ionic currents through hSlo1 Y318S at four different voltages (blue, control; red, DHA). (B) Fractional changes in peak outward currents through hSlo1 Y318S by DHA. $n = 16$. (C) G-V curves before (blue) and after (red) the application of DHA. $n = 16$. (D) Changes in $V_{0.5}$ (left) and Q_{app} (right) in individual experiments. Neither changes are significant (P = 0.10 and 0.32). (E) Normalized currents through hSlo1 Y318S before (blue) and after (red) the application of DHA at three different voltages from a representative patch. (F) Voltage dependence of time constant of current relaxation before (blue) and after (red) the application of DHA. $n = 10$–16. (G) Fractional changes in time constant of current relaxation by DHA. $n = 10$–16. (H) DHA at 3 and 10 μM fails to increase currents through hSlo1 Y318S. Currents were elicited by pulses to 130 mV ($G/G_{max} = \sim 0.15$), and the peak outward current sizes are plotted. All results were obtained without intracellular Ca^{2+}, and, except where indicated, DHA was applied at 3 μM.

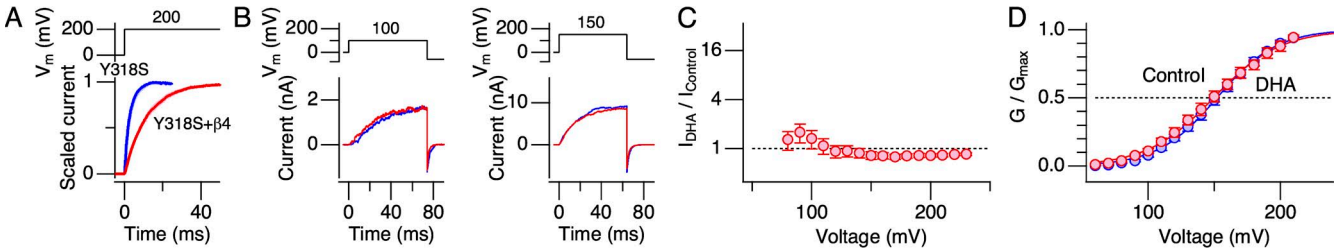

Figure 12. DHA fails to alter currents through hSlo1 Y318S+hβ4. (A) Comparison of the activation kinetics of the currents obtained from cells transfected with the hSlo1 Y318S DNA (blue) and the hSlo1 Y318S and hβ4 DNAs together (red). $n = 16$ and 8 for hSlo1 Y318S and hSlo1 Y318S+hβ4, respectively. The line width indicates SEM. (B) Representative currents measured at two different voltages before (blue) and after (red) the application of DHA. (C) Fractional increases in peak outward currents by DHA. $n = 8$. (D) G-V curves before (blue) and after (red) the application of DHA. $n = 6$. The smooth curves are Boltzmann fits to the results. The estimated $V_{0.5}$ and Q_{app} values for the control group are 152.2 ± 0.8 mV and 1.11 ± 0.04, and for the DHA group are 149.5 ± 1.1 mV and 1.00 ± 0.04 ($n = 6$). DHA was applied at 3 µM. All results were obtained without intracellular Ca^{2+}.

et al., 2013c). In both hSlo1 and hSlo1+hβ1, DHA increases P_o at very negative voltages in the virtual absence of Ca^{2+}. Thus, DHA most probably increases L_0, which reflects the closed–open equilibrium of the ion conduction gate in the model of Horrigan and Aldrich (2002) ("HA model"), consequently shifting macroscopic G-V to the negative direction in a relatively Ca^{2+}-independent manner. Of the two rate constants contributing to L_0, we propose that DHA predominantly increases the forward closed-to-open rate constant (δ_0 in the HA model) at extreme negative voltages where the VSDs are at rest, because the mean open durations at such voltages are not appreciably altered. If similar changes are maintained when the VSDs of the channel are activated ($\delta_{1–4}$ in the HA model), it would account for the acceleration of the activation kinetics by DHA at intermediate voltages in both hSlo1 and hSlo1+hβ1. At very positive voltages where G/G_{max} is nearly saturated, the activation kinetics is not significantly faster with DHA (Fig. 1, F and G) (Hoshi et al., 2013b,c); the effects of DHA on the forward rate constants may not be uniform, and may depend on activation of the VSDs. It should be noted that the confidence on the estimate of the effect of DHA on L_0 may be somewhat limited by the brief nature of the channel openings at extreme negative voltages, often ∼100 µs (Fig. 2). Furthermore, our measurements do not necessarily preclude any action of DHA on other aspects of the Slo1 channel, such as the VSD function, although we expect it to be relatively minor if any. The underlying biophysical mechanisms may be similar qualitatively; however, DHA clearly exerts a much greater effect in hSlo1+hβ1 than in hSlo1 alone. In hSlo1+hβ1, the P_o values at negative voltages without Ca^{2+} increase by >20-fold (Hoshi et al., 2013c), but the increases are limited only to approximately threefold in hSlo1 alone. Thus, as proposed earlier (Hoshi et al., 2013c), coexpression of hβ1 may be considered to "amplify" the functional

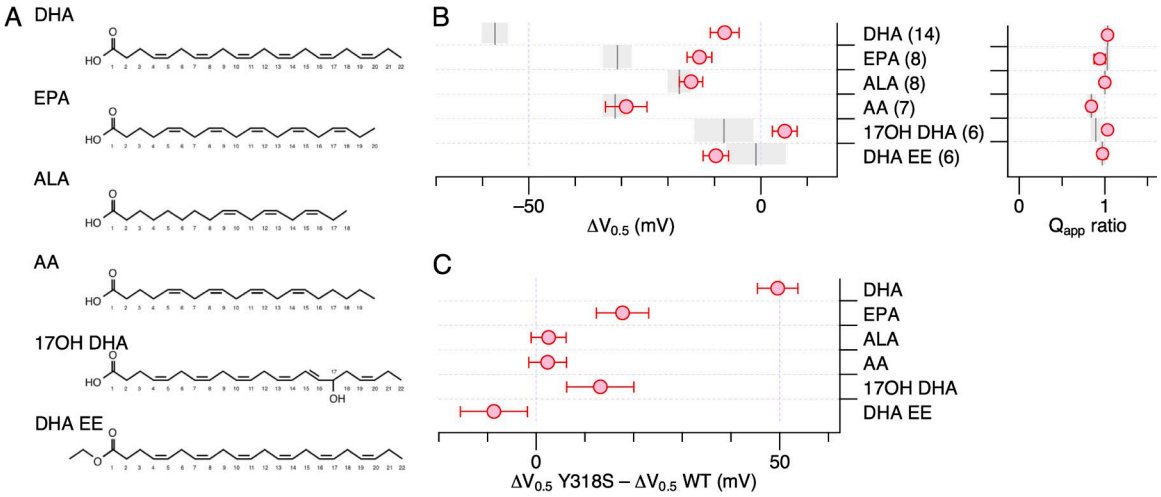

Figure 13. Sensitivities of hSlo1 Y318S+hβ1 complexes to various fatty acids. (A) Fatty acid structures. DHA (22:6(ω-3)), EPA (20:5(ω-3)), ALA (18:3(ω-3)), AA (20:4(ω-6)), 17OH DHA, and DHA EE. (B) Changes in G-V $V_{0.5}$ (left) and fractional changes in Q_{app} (right) by the fatty acids indicated. The vertical line and the surrounding gray area for each reagent represent the mean ± SEM response from the wild-type hSlo1+hβ1 complex. When corrected for five-way comparisons, the $\Delta V_{0.5}$ values of hSlo1 Y318S+hβ1 for DHA and those for EPA significantly differ from those of wild-type hSlo1+hβ1 for DHA ($P < 10^{-7}$ and 0.02, respectively). (C) Differences in $\Delta V_{0.5}$ between hSlo1 Y318S+hβ1 and wild-type hSlo1+hβ1 caused by the fatty acids indicated.

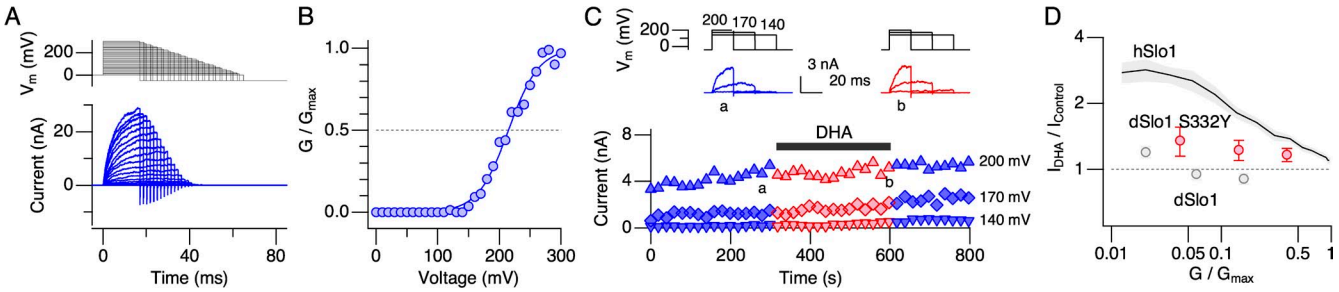

Figure 14. The *Drosophila*-to-human mutation S332Y in dSlo1 does not introduce any noticeable DHA sensitivity. (A) Representative currents through dSlo1 S332Y elicited by pulses to different voltages. (B) A representative G-V curve. The smooth curve represents a Boltzmann fit to the results. The $V_{0.5}$ and Q_{app} values are 214.8 ± 2.7 mV and 1.01 ± 0.10. (C) Peak outward currents at three different voltages as a function of time. 3 µM DHA was applied during the time indicated by the black bar. Representative currents before (blue) and after (red) the application of DHA are also shown (top). (D) Fractional changes in peak outward currents at different G/G_{max} values in dSlo1 S332Y (red). The results obtained at 140, 170, and 200 mV were transformed using the G-V information shown in B. $n = 7$. For comparison, the results obtained from hSlo1 and dSlo1 are also shown.

consequences of the interaction of DHA with the hSlo1 protein itself. The physicochemical nature of this amplification process remains to be investigated, but our previous study shows that a possible electrostatic interaction in the N terminus of some hβ subunits is critical (Hoshi et al., 2013b). Our measurements thus demonstrate that the principal effector of DHA is the ion conduction gate of the hSlo1 BK channel. In Shaker K^+ channels, however, DHA (at >10 µM) electrostatically interacts with the VSDs (Börjesson et al., 2008); the effects of DHA may vary depending on the channel type.

The lack of responsiveness to DHA of Slo1 channels from *Drosophila*, which does not normally contain DHA in the body (Shen et al., 2010), has allowed us to deploy a chimeric strategy to identify the molecular component critical for the differential effects of DHA on dSlo1 and hSlo1 channels. Mutation of Y318 located most probably at the cytoplasmic end of S6 in hSlo1 to S, as found in dSlo1, impairs the response to DHA in hSlo1, hSlo1+hβ1, and hSlo1+hβ4. Our results did not identify any other statistically significant contributions. Importantly, in the absence of DHA, the gating characteristics of the mutant channel complexes containing the mutation Y318S otherwise closely resemble those of the wild-type channels. The observation that Y318 in S6, near the ion conduction gate located somewhere near the selectivity filter (Wilkens and Aldrich, 2006; Tang et al., 2010; Chen and Aldrich, 2011; Zhou et al., 2011; Thompson and Begenisich, 2012), plays

TABLE 1

*Boltzmann fit parameters for the hSlo1+hβ1 complexes with human-to-*Drosophila *mutations*

Segment	Mutation	Control		3 µM DHA		
		$V_{0.5}$	Q_{app}	$V_{0.5}$	Q_{app}	*n*
		mV		*mV*		
S5	V236A	110.8 ± 1.1	1.10 ± 0.05	62.8 ± 2.7	1.10 ± 0.11	6
S5	N237Q	208.8 ± 0.8	0.95 ± 0.03	162.2 ± 1.3	0.87 ± 0.04	6
S5	L239V	144.3 ± 1.3	1.02 ± 0.05	93.6 ± 2.4	0.91 ± 0.07	8
S5	T245V	130.5 ± 1.0	1.13 ± 0.04	79.7 ± 1.4	1.14 ± 0.06	8
S5	F252I	235.7 ± 1.0	0.81 ± 0.04	184.2 ± 1.2	0.66 ± 0.02	6
P/filter	L280F	99.6 ± 1.9	0.90 ± 0.06	51.0 ± 1.8	0.89 ± 0.05	6
P/filter	M282I	290.4 ± 6.5	0.52 ± 0.07	195.4 ± 1.8	0.74 ± 0.04	7
P/filter	A295C	187.4 ± 1.2	0.84 ± 0.04	129.4 ± 2.3	0.84 ± 0.06	6
P/filter	K296E	163.3 ± 1.1	0.88 ± 0.03	110.8 ± 1.9	0.86 ± 0.05	6
P/filter	T298V	163.9 ± 1.1	0.90 ± 0.03	112.4 ± 1.5	0.92 ± 0.04	6
S6	L302T	146.8 ± 2.3	0.85 ± 0.06	92.9 ± 2.5	0.87 ± 0.07	6
S6	M304L	175.6 ± 1.5	0.75 ± 0.03	127.7 ± 1.8	0.78 ± 0.04	6
S6	I308L:G310V	155.2 ± 1.3	0.84 ± 0.03	117.1 ± 2.8	0.85 ± 0.06	8
S6	Y318S	159.1 ± 1.2	0.79 ± 0.03	152.4 ± 1.2	0.75 ± 0.03	14
S6	V319I	195.4 ± 0.9	0.90 ± 0.03	147.4 ± 1.6	0.79 ± 0.04	8
S6	I326V	184.7 ± 1.5	0.78 ± 0.04	129.9 ± 3.0	0.76 ± 0.06	6

All results were obtained in the absence of intracellular Ca^{2+}. In each construct, the values estimated from the individual experiments were pooled and fit with the Boltzmann function.

a critical role may be consistent with the conclusion of the biophysical measurements that DHA alters the equilibrium constant L_0 in the HA model, representing the intrinsic stability of the ion conduction gate. The converse mutation S332Y in dSlo1 fails to introduce any DHA sensitivity to dSlo1; multiple structural components must be missing in the gating machinery of dSlo1 to respond to DHA.

It is clear that the mutation Y318S impairs the response of the hSlo1 channel to DHA. However, the results presented here do not specify the exact functional role of Y318 in the DHA sensitivity of hSlo1. This residue could be a structural component of the DHA-binding site itself or a component of the coupling mechanism that bridges the binding site located elsewhere to the effector site, probably the ion conduction gate near the ion selectivity filter (Wilkens and Aldrich, 2006; Tang et al., 2010; Chen and Aldrich, 2011; Zhou et al., 2011; Thompson and Begenisich, 2012). A similar interpretational issue was raised by Zhou et al. (2010) regarding the role of hSlo1 G311 in mediating the inhibitory effect of paxilline, a tremogenic alkaloid, on the Slo1 channel. An experimentally determined atomic structure of the Slo1 transmembrane domain is not yet available, and homology models based on the Kv1.2/2.1 structure may be of limited usefulness (Zhou et al., 2011); thus, the exact location of Y318 in hSlo1 is unknown. However, based on its location in the primary structure, Y318 is expected to be near the C-terminal end of S6 and may be exposed to the cytoplasmic side such that DHA can gain access to the residue through the narrow gap between the transmembrane domain and the cytoplasmic gating ring domain (Yang et al., 2008, 2013). Alternatively, it is conceivable that the Slo1 channel could have lateral openings through the transmembrane segments as found in voltage-independent two-pore domain K^+ channels (Brohawn et al., 2012; Miller and Long, 2012), which are modulated by AA (Fink et al., 1998), and also in the bacterial Na^+ channel NavAb (Payandeh et al., 2011). It is interesting to note that Y318 is three and six residues away from F315 and L312, respectively, which together may mediate coupling of the ion conduction gate with the Ca^{2+} sensors (Wu et al., 2009).

A particularly interesting effect of the human-to-*Drosophila* mutation Y318S is that the response of hSlo1 Y318S+hβ1 to DHA is virtually eliminated, but those to other fatty acids, such as the shorter omega-3 fatty acid ALA and also the omega-6 fatty acid AA, remain unaltered. Thus, it may be interpreted that the mutation Y318S alters the stimulus rank order of the hSlo1+hβ1 channel complex and probably that of the hSlo1 channel without any auxiliary subunit. In wild-type channels, the stimulus rank order based on the mean $\Delta V_{0.5}$ values is DHA > AA = EPA > ALA > 17OH DHA > DHA EE. With Y318S, the order changes to AA > ALA = EPA > DHA EE > DHA > 17OH DHA. Changes in the stimulus/ligand rank order are often observed when binding sites themselves are altered (e.g., Drake et al., 1997). Therefore, the altered rank order observed in this study may suggest that hSlo1 Y318 is within or near the free fatty-acid sensor of the hSlo1 channel. The Y318S-independent effect of AA probably represents the same phenomenon reported by Clarke et al. (2002) using native channel complexes from pulmonary smooth muscles cells, most probably Slo1+β1.

Crystal structures of some proteins with DHA bound are available: for example, brain fatty acid–binding protein (Protein Data Bank accession no. 1FDQ; Balendiran et al., 2000), nuclear retinoid X receptor (Protein Data Bank accession no. 1MV9; Egea et al., 2002), and cyclooxygenase-2 (Protein Data Bank accession no. 3HS7; Vecchio et al., 2010). None of these proteins are transmembrane proteins, and how relevant they are to Slo1 is unclear. Nevertheless, DHA in these structures assumes a semicircular omega shape, and the carboxylic acid head group interacts with the side chain of an arginine (Protein Data Bank accession no. 1MV9; Egea et al., 2002) or of a tyrosine (Protein Data Bank accession nos. 1FDQ and 3HS7; Vecchio et al., 2010). Thus, the idea that hSlo1 Y318 directly interacts with DHA may be feasible.

The observation that the response of hSlo1+hβ1 to AA, an omega-6 fatty acid, is unaltered by the mutation Y318S could be explained at least in two ways. First, AA may bind to the same site as DHA, but the mutation Y318S somehow does not interfere with the AA-induced conformational change. Second, AA may increase the channel activity through a different mechanism unaltered by the mutation Y318S. These possibilities are not well discriminated by the results presented here, but our observations clearly illustrate the complexity of lipid-based modulation.

Although the direct action of free DHA on the hSlo1 channel complex critically depends on hSlo1 Y318, DHA probably exerts other effects on the channel complex independently of Y318. As suggested by the current-diminishing effect of 10 µM DHA on hSlo1 Y318S, DHA may inhibit or block the channel at higher concentrations. Inhibitory effects of free fatty acids at micromolar levels were also observed in other K^+ channels (Guizy et al., 2005). Additionally, DHA is capable of regulating native BK channel complexes indirectly through its metabolic breakdown products involving the enzyme cytochrome P450 epoxygenase (Ye et al., 2002; Lai et al., 2009; Wang et al., 2011). One of the challenges is therefore to identify and delineate the multiple lipid-based pathways converging on BK channel complexes.

In summary, our study demonstrates that DHA facilitates opening of the ion conduction gate of the Slo1 BK channel, and that a single residue at the cytoplasmic end of S6 accounts for the differential effects of DHA on hSlo1 and dSlo1. The human-to-*Drosophila* mutation Y318S impairs the direct current enhancing effect of DHA and EPA preferentially and represents an excellent tool to dissect out the complex molecular mechanisms underlying modulation of BK channels by fatty acids.

This work was supported by the public in part through the National Institutes of Health (R01GM057654), German Research Foundation (DFG, HE 2993/8), National Natural Science Foundation of China (31271217), and the Key Project of Shanghai Science and Technology Commission (contract no. 11JC1406400). The authors declare no conflict of interest.

Kenton J. Swartz served as editor.

Submitted: 12 July 2013
Accepted: 23 September 2013

REFERENCES

Avdonin, V., X.D. Tang, and T. Hoshi. 2003. Stimulatory action of internal protons on Slo1 BK channels. *Biophys. J.* 84:2969–2980. http://dx.doi.org/10.1016/S0006-3495(03)70023-X

Balendiran, G.K., F. Schnutgen, G. Scapin, T. Borchers, N. Xhong, K. Lim, R. Godbout, F. Spener, and J.C. Sacchettini. 2000. Crystal structure and thermodynamic analysis of human brain fatty acid-binding protein. *J. Biol. Chem.* 275:27045–27054.

Börjesson, S.I., S. Hammarström, and F. Elinder. 2008. Lipoelectric modification of ion channel voltage gating by polyunsaturated fatty acids. *Biophys. J.* 95:2242–2253. http://dx.doi.org/10.1529/biophysj.108.130757

Brasky, T.M., A.K. Darke, X. Song, C.M. Tangen, P.J. Goodman, I.M. Thompson, F.L. Meyskens Jr., G.E. Goodman, L.M. Minasian, H.L. Parnes, et al. 2013. Plasma phospholipid fatty acids and prostate cancer risk in the SELECT trial. *J. Natl. Cancer Inst.* 105:1132–1141. http://dx.doi.org/10.1093/jnci/djt174

Brenner, R., T.J. Jegla, A. Wickenden, Y. Liu, and R.W. Aldrich. 2000a. Cloning and functional characterization of novel large conductance calcium-activated potassium channel β subunits, hKCNMB3 and hKCNMB4. *J. Biol. Chem.* 275:6453–6461. http://dx.doi.org/10.1074/jbc.275.9.6453

Brenner, R., G.J. Peréz, A.D. Bonev, D.M. Eckman, J.C. Kosek, S.W. Wiler, A.J. Patterson, M.T. Nelson, and R.W. Aldrich. 2000b. Vasoregulation by the β1 subunit of the calcium-activated potassium channel. *Nature.* 407:870–876. http://dx.doi.org/10.1038/35038011

Brohawn, S.G., J. del Mármol, and R. MacKinnon. 2012. Crystal structure of the human K2P TRAAK, a lipid- and mechano-sensitive K^+ ion channel. *Science.* 335:436–441. http://dx.doi.org/10.1126/science.1213808

Chen, X., and R.W. Aldrich. 2011. Charge substitution for a deep-pore residue reveals structural dynamics during BK channel gating. *J. Gen. Physiol.* 138:137–154. http://dx.doi.org/10.1085/jgp.201110632

Clarke, A.L., S. Petrou, J.V. Walsh Jr., and J.J. Singer. 2002. Modulation of BK_{Ca} channel activity by fatty acids: structural requirements and mechanism of action. *Am. J. Physiol. Cell Physiol.* 283:C1441–C1453. http://dx.doi.org/10.1152/ajpcell.00035.2002

Drake, S.K., M.A. Zimmer, C. Kundrot, and J.J. Falke. 1997. Molecular tuning of an EF-hand-like calcium binding loop. Contributions of the coordinating side chain at loop position 3. *J. Gen. Physiol.* 110:173–184. http://dx.doi.org/10.1085/jgp.110.2.173

Egea, P.F., A. Mitschler, and D. Moras. 2002. Molecular recognition of agonist ligands by RXRs. *Mol. Endocrinol.* 16:987–997. http://dx.doi.org/10.1210/me.16.5.987

Fink, M., F. Lesage, F. Duprat, C. Heurteaux, R. Reyes, M. Fosset, and M. Lazdunski. 1998. A neuronal two P domain K^+ channel stimulated by arachidonic acid and polyunsaturated fatty acids. *EMBO J.* 17:3297–3308. http://dx.doi.org/10.1093/emboj/17.12.3297

Flock, M.R., C.J. Rogers, K.S. Prabhu, and P.M. Kris-Etherton. 2013. Immunometabolic role of long-chain omega-3 fatty acids in obesity-induced inflammation. *Diabetes Metab. Res. Rev.* 29:431–445. http://dx.doi.org/10.1002/dmrr.2414

Guizy, M., C. Arias, M. David, T. González, and C. Valenzuela. 2005. Ω-3 and Ω-6 polyunsaturated fatty acids block HERG channels. *Am. J. Physiol. Cell Physiol.* 289:C1251–C1260. http://dx.doi.org/10.1152/ajpcell.00036.2005

Horrigan, F.T., and R.W. Aldrich. 2002. Coupling between voltage sensor activation, Ca^{2+} binding and channel opening in large conductance (BK) potassium channels. *J. Gen. Physiol.* 120:267–305. http://dx.doi.org/10.1085/jgp.20028605

Horrigan, F.T., J. Cui, and R.W. Aldrich. 1999. Allosteric voltage gating of potassium channels I. Mslo ionic currents in the absence of Ca^{2+}. *J. Gen. Physiol.* 114:277–304. http://dx.doi.org/10.1085/jgp.114.2.277

Horrigan, F.T., S.H. Heinemann, and T. Hoshi. 2005. Heme regulates allosteric activation of the Slo1 BK channel. *J. Gen. Physiol.* 126:7–21. http://dx.doi.org/10.1085/jgp.200509262

Horrocks, L.A., and A.A. Farooqui. 2004. Docosahexaenoic acid in the diet: its importance in maintenance and restoration of neural membrane function. *Prostaglandins Leukot. Essent. Fatty Acids.* 70:361–372. http://dx.doi.org/10.1016/j.plefa.2003.12.011

Hoshi, T., A. Pantazis, and R. Olcese. 2013a. Transduction of voltage and Ca^{2+} signals by Slo1 BK channels. *Physiology (Bethesda).* 28:172–189. http://dx.doi.org/10.1152/physiol.00055.2012

Hoshi, T., Y. Tian, R. Xu, S.H. Heinemann, and S. Hou. 2013b. Mechanism of the modulation of BK potassium channel complexes with different auxiliary subunit compositions by the omega-3 fatty acid DHA. *Proc. Natl. Acad. Sci. USA.* 110:4822–4827. http://dx.doi.org/10.1073/pnas.1222003110

Hoshi, T., B. Wissuwa, Y. Tian, N. Tajima, R. Xu, M. Bauer, S.H. Heinemann, and S. Hou. 2013c. Omega-3 fatty acids lower blood pressure by directly activating large-conductance Ca^{2+}-dependent K^+ channels. *Proc. Natl. Acad. Sci. USA.* 110:4816–4821. http://dx.doi.org/10.1073/pnas.1221997110

Hou, S.W., S.H. Heinemann, and T. Hoshi. 2009. Modulation of BK_{Ca} channel gating by endogenous signaling molecules. *Physiology (Bethesda).* 24:26–35. http://dx.doi.org/10.1152/physiol.00032.2008

Ichimura, A., A. Hirasawa, O. Poulain-Godefroy, A. Bonnefond, T. Hara, L. Yengo, I. Kimura, A. Leloire, N. Liu, K. Iida, et al. 2012. Dysfunction of lipid sensor GPR120 leads to obesity in both mouse and human. *Nature.* 483:350–354. http://dx.doi.org/10.1038/nature10798

Im, D.S. 2012. Omega-3 fatty acids in anti-inflammation (pro-resolution) and GPCRs. *Prog. Lipid Res.* 51:232–237. http://dx.doi.org/10.1016/j.plipres.2012.02.003

Knaus, H.G., K. Folander, M. Garcia-Calvo, M.L. Garcia, G.J. Kaczorowski, M. Smith, and R. Swanson. 1994. Primary sequence and immunological characterization of β-subunit of high conductance Ca^{2+}-activated K^+ channel from smooth muscle. *J. Biol. Chem.* 269:17274–17278.

Lai, L.H., R.X. Wang, W.P. Jiang, X.J. Yang, J.P. Song, X.R. Li, and G. Tao. 2009. Effects of docosahexaenoic acid on large-conductance Ca^{2+}-activated K^+ channels and voltage-dependent K^+ channels in rat coronary artery smooth muscle cells. *Acta Pharmacol. Sin.* 30:314–320. http://dx.doi.org/10.1038/aps.2009.7

Lauritzen, L., H.S. Hansen, M.H. Jørgensen, and K.F. Michaelsen. 2001. The essentiality of long chain n-3 fatty acids in relation to development and function of the brain and retina. *Prog. Lipid Res.* 40:1–94. http://dx.doi.org/10.1016/S0163-7827(00)00017-5

Liu, J.C., S.M. Conklin, S.B. Manuck, J.K. Yao, and M.F. Muldoon. 2011. Long-chain omega-3 fatty acids and blood pressure. *Am. J. Hypertens.* 24:1121–1126. http://dx.doi.org/10.1038/ajh.2011.120

Meera, P., M. Wallner, and L. Toro. 2000. A neuronal β subunit (KCNMB4) makes the large conductance, voltage- and Ca^{2+}-activated K^+ channel resistant to charybdotoxin and iberiotoxin. *Proc. Natl.*

Acad. Sci. USA. 97:5562–5567. http://dx.doi.org/10.1073/pnas.100118597

Miller, A.N., and S.B. Long. 2012. Crystal structure of the human two-pore domain potassium channel K2P1. *Science.* 335:432–436. http://dx.doi.org/10.1126/science.1213274

Mozaffarian, D., and J.H. Wu. 2011. Omega-3 fatty acids and cardiovascular disease: effects on risk factors, molecular pathways, and clinical events. *J. Am. Coll. Cardiol.* 58:2047–2067. http://dx.doi.org/10.1016/j.jacc.2011.06.063

Nelson, M.T., and J.M. Quayle. 1995. Physiological roles and properties of potassium channels in arterial smooth muscle. *Am. J. Physiol.* 268:C799–C822.

Oh, D.Y., S. Talukdar, E.J. Bae, T. Imamura, H. Morinaga, W. Fan, P. Li, W.J. Lu, S.M. Watkins, and J.M. Olefsky. 2010. GPR120 is an omega-3 fatty acid receptor mediating potent anti-inflammatory and insulin-sensitizing effects. *Cell.* 142:687–698. http://dx.doi.org/10.1016/j.cell.2010.07.041

Orr, S.K., M.O. Trépanier, and R.P. Bazinet. 2013. n-3 Polyunsaturated fatty acids in animal models with neuroinflammation. *Prostaglandins Leukot. Essent. Fatty Acids.* 88:97–103. http://dx.doi.org/10.1016/j.plefa.2012.05.008

Payandeh, J., T. Scheuer, N. Zheng, and W.A. Catterall. 2011. The crystal structure of a voltage-gated sodium channel. *Nature.* 475:353–358. http://dx.doi.org/10.1038/nature10238

Ramel, A., J.A. Martinez, M. Kiely, N.M. Bandarra, and I. Thorsdottir. 2010. Moderate consumption of fatty fish reduces diastolic blood pressure in overweight and obese European young adults during energy restriction. *Nutrition.* 26:168–174. http://dx.doi.org/10.1016/j.nut.2009.04.002

Rizos, E.C., E.E. Ntzani, E. Bika, M.S. Kostapanos, and M.S. Elisaf. 2012. Association between omega-3 fatty acid supplementation and risk of major cardiovascular disease events: a systematic review and meta-analysis. *JAMA.* 308:1024–1033. http://dx.doi.org/10.1001/2012.jama.11374

Roncaglioni, M.C., M. Tombesi, F. Avanzini, S. Barlera, V. Caimi, P. Longoni, I. Marzona, V. Milani, M.G. Silletta, G. Tognoni, and R. Marchioli; Risk and Prevention Study Collaborative Group. 2013. n-3 fatty acids in patients with multiple cardiovascular risk factors. *N. Engl. J. Med.* 368:1800–1808. http://dx.doi.org/10.1056/NEJMoa1205409

Saravanan, P., N.C. Davidson, E.B. Schmidt, and P.C. Calder. 2010. Cardiovascular effects of marine omega-3 fatty acids. *Lancet.* 376:540–550. http://dx.doi.org/10.1016/S0140-6736(10)60445-X

Schopperle, W.M., M.H. Holmqvist, Y. Zhou, J. Wang, Z. Wang, L.C. Griffith, I. Keselman, F. Kusinitz, D. Dagan, and I.B. Levitan. 1998. Slob, a novel protein that interacts with the Slowpoke calcium-dependent potassium channel. *Neuron.* 20:565–573. http://dx.doi.org/10.1016/S0896-6273(00)80995-2

Shen, L.R., C.Q. Lai, X. Feng, L.D. Parnell, J.B. Wan, J.D. Wang, D. Li, J.M. Ordovas, and J.X. Kang. 2010. *Drosophila* lacks C20 and C22 PUFAs. *J. Lipid Res.* 51:2985–2992. http://dx.doi.org/10.1194/jlr.M008524

Sun, X., D. Zhou, P. Zhang, E.G. Moczydlowski, and G.G. Haddad. 2007. β-subunit-dependent modulation of *hSlo* BK current by arachidonic acid. *J. Neurophysiol.* 97:62–69. http://dx.doi.org/10.1152/jn.00700.2006

Tang, Q.Y., Z. Zhang, X.M. Xia, and C.J. Lingle. 2010. Block of mouse Slo1 and Slo3 K^+ channels by CTX, IbTX, TEA, 4-AP and quinidine. *Channels (Austin).* 4:22–41. http://dx.doi.org/10.4161/chan.4.1.10481

Thompson, J., and T. Begenisich. 2012. Selectivity filter gating in large-conductance Ca^{2+}-activated K^+ channels. *J. Gen. Physiol.* 139:235–244. http://dx.doi.org/10.1085/jgp.201110748

Uauy, R., and A.D. Dangour. 2006. Nutrition in brain development and aging: role of essential fatty acids. *Nutr. Rev.* 64:S24–S33. http://dx.doi.org/10.1301/nr.2006.may.S24-S33

Vaithianathan, T., A. Bukiya, J. Liu, P. Liu, M. Asuncion-Chin, Z. Fan, and A. Dopico. 2008. Direct regulation of BK channels by phosphatidylinositol 4,5-bisphosphate as a novel signaling pathway. *J. Gen. Physiol.* 132:13–28. http://dx.doi.org/10.1085/jgp.200709913

Vecchio, A.J., D.M. Simmons, and M.G. Malkowski. 2010. Structural basis of fatty acid substrate binding to cyclooxygenase-2. *J. Biol. Chem.* 285:22152–22163. http://dx.doi.org/10.1074/jbc.M110.119867

Wallner, M., P. Meera, M. Ottolia, G.J. Kaczorowski, R. Latorre, M.L. Garcia, E. Stefani, and L. Toro. 1995. Characterization of and modulation by a β-subunit of a human maxi K_{Ca} channel cloned from myometrium. *Receptors Channels.* 3:185–199.

Wang, R.X., Q. Chai, T. Lu, and H.C. Lee. 2011. Activation of vascular BK channels by docosahexaenoic acid is dependent on cytochrome P450 epoxygenase activity. *Cardiovasc. Res.* 90:344–352. http://dx.doi.org/10.1093/cvr/cvq411

Wilkens, C.M., and R.W. Aldrich. 2006. State-independent block of BK channels by an intracellular quaternary ammonium. *J. Gen. Physiol.* 128:347–364. http://dx.doi.org/10.1085/jgp.200609579

Wu, Y., Y. Xiong, S. Wang, H. Yi, H. Li, N. Pan, F.T. Horrigan, Y. Wu, and J. Ding. 2009. Intersubunit coupling in the pore of BK channels. *J. Biol. Chem.* 284:23353–23363. http://dx.doi.org/10.1074/jbc.M109.027789

Yan, Y., W. Jiang, T. Spinetti, A. Tardivel, R. Castillo, C. Bourquin, G. Guarda, Z. Tian, J. Tschopp, and R. Zhou. 2013. Omega-3 fatty acids prevent inflammation and metabolic disorder through inhibition of NLRP3 inflammasome activation. *Immunity.* 38:1154–1163. http://dx.doi.org/10.1016/j.immuni.2013.05.015

Yang, H., J. Shi, G. Zhang, J. Yang, K. Delaloye, and J. Cui. 2008. Activation of Slo1 BK channels by Mg^{2+} coordinated between the voltage sensor and RCK1 domains. *Nat. Struct. Mol. Biol.* 15:1152–1159. http://dx.doi.org/10.1038/nsmb.1507

Yang, J., H. Yang, X. Sun, K. Delaloye, X. Yang, A. Moller, J. Shi, and J. Cui. 2013. Interaction between residues in the Mg^{2+}-binding site regulates BK channel activation. *J. Gen. Physiol.* 141:217–228. http://dx.doi.org/10.1085/jgp.201210794

Ye, D., D. Zhang, C. Oltman, K. Dellsperger, H.C. Lee, and M. VanRollins. 2002. Cytochrome p-450 epoxygenase metabolites of docosahexaenoate potently dilate coronary arterioles by activating large-conductance calcium-activated potassium channels. *J. Pharmacol. Exp. Ther.* 303:768–776. http://dx.doi.org/10.1124/jpet.303.2.768

Yon, J., and M. Fried. 1989. Precise gene fusion by PCR. *Nucleic Acids Res.* 17:4895. http://dx.doi.org/10.1093/nar/17.12.4895

Zhou, Y., Q.Y. Tang, X.M. Xia, and C.J. Lingle. 2010. $Glycine_{311}$, a determinant of paxilline block in BK channels: A novel bend in the BK S6 helix. *J. Gen. Physiol.* 135:481–494. http://dx.doi.org/10.1085/jgp.201010403

Zhou, Y., X.M. Xia, and C.J. Lingle. 2011. Cysteine scanning and modification reveal major differences between BK channels and Kv channels in the inner pore region. *Proc. Natl. Acad. Sci. USA.* 108:12161–12166. http://dx.doi.org/10.1073/pnas.1104150108